Understanding the dynamic evolution of cyclic variability at the operating limits of HCCI engines with negative valve overlap

Erik Hellström, Anna Stefanopoulou, Jiri Vavra, Aristotelis Babajimopoulos, and Dennis Assanis
University of Michigan

Li Jiang and Hakan Yilmaz
Robert Bosch LLC

ABSTRACT

An experimental study is performed for homogeneous charge compression ignition (HCCI) combustion focusing on late phasing conditions with high cyclic variability (CV) approaching misfire. High CV limits the feasible operating range and the objective is to understand and quantify the dominating effects of the CV in order to enable controls for widening the operating range of HCCI. A combustion analysis method is developed for explaining the dynamic coupling in sequences of combustion cycles where important variables are residual gas temperature, combustion efficiency, heat release during re-compression, and unburned fuel mass. The results show that the unburned fuel mass carries over to the re-compression and to the next cycle creating a coupling between cycles, in addition to the well known temperature coupling, that is essential for understanding and predicting the HCCI behavior at lean conditions with high CV.

INTRODUCTION

It was early noted that homogeneous charge compression ignition (HCCI) combustion can have low cyclic variability (CV) compared to spark ignited (SI) combustion [1]. However, at certain operating conditions, even if all inputs are held constant, the combustion phasing can alternate between early and late timing in a oscillatory manner or run away towards increasingly advanced conditions. The process can exhibit significant oscillations at late phasing [2, 3] and runaway-knock phenomena at high loads [4]. This behavior points to the fact that there is considerable nonlinear feedback between cycles that can stabilize or destabilize the process. The coupling has been attributed to the fast variations from cycle to cycle in combustion inefficiency and residual gas temperature [5, 6] and the slower variation of the cylinder wall temperature [4, 7, 8].

HCCI can be achieved with variable valve timing and the focus here is on the negative valve overlap (nvo) strategy. This re-compression strategy is also known as controlled autoigni-tion (CAI) and means that autoignition is induced by raising the charge temperature of the next cycle by trapping and compressing residual gases from earlier cycles through an early closing of the exhaust valve [9].

To investigate the nature of CV, we perform a set of experiments and then analyze the data in order to arrive at an interpretation of the dynamical behavior of the process. To enable the analysis, standard combustion analysis methods are extended with a novel method for determining the unburned fuel mass and combustion efficiency on cycle basis. The main contribution in our work is this thermodynamic analysis of the experimental data which explains and quantifies the dominating effects governing the process. Specifically, the analysis show that lean HCCI combustion with high CV is mainly the result of the recycled thermal energy in the residual gas and the unburned fuel passing over to the re-compression and to the next cycle.

Experiments with the re-compression strategy at conditions with noticeable CV were performed and analyzed in [5, 10]. Linear correlation coefficients were also computed to study the relationships between subsequent cycles. Control of valve timings and injection timings for reducing the CV was developed in [11, 12] based on model linearizations. Our analysis corroborate the trends found in [5, 10] and used in [11, 12] but also show that, for high CV, the relationships are more complicated than can be captured with a linear analysis. Specifically, there are sequences of cycles, characterized by combustion phasing and heat release, that occurs with increasing probability when the CV increases.

The focus here is on understanding lean HCCI combustion operated with nvo. Wagner et al. [13, 14] report experimental observations and analysis of transitions, using variable valve timing, between SI and spark-assisted HCCI combustion with stoichiometric mixtures where the process transitions through regions with high CV. These conditions give qualitatively different dynamical behavior than the lean case without spark assist.

HCCI engines operating with intake heating and a low amount of residuals also show different behavior, as shown in [15].

Experimental work investigating the effect of different mixtures of primary reference fuels on CV in HCCI are found in [16–18]. An analysis of the stability of HCCI with large amounts of residual gas was done in [19] where, by studying the thermal dynamics of the charge, unstable behavior with limit cycles at late phasing and runaway knock at early phasing were predicted. Similar analysis is also shown in [20]. Our work show that, for higher CV, the effect of unburned fuel creates an additional coupling that must be taken into account. The use of injecting fuel during the nvo period for control was mentioned in [9] and experimentally investigated in [21, 22] and used in [23, 24] to extend the low load limit of HCCI. In the present work, the injection parameters are constant for each operating point and the effect of the unburned fuel, recycled from incomplete combustion in previous cycles, is investigated.

The objective here is to identify, understand, and quantify the most influential properties for the CV to enable control-oriented modeling. A simulation model for studying misfire in HCCI using chemical kinetics with 31 species and air flow model was developed in [25] and reduced to a eight state model in [26]. Our aim is to find the dominant factors and a minimum set of variables for describing CV.

The paper is organized as follows. The experimental setup is described first and the data analysis method used is outlined. After that, the results from the methodology are interpreted in order to explain the dynamic behavior of the combustion process. Finally, the conclusions from the work are summarized.

EXPERIMENTAL SETUP

Experiments were performed at the Automotive Laboratory at University of Michigan on a single-cylinder gasoline direct-injected engine with a Ricardo Hydra crankcase. The engine is equipped with an electro-hydraulic fully-flexible valve actuation (FFVA) system from Sturman Industries, which allows lift, timing, and duration of each valve event to be controlled independently. Fuel is delivered via a gasoline injector mounted between the two intake valves and aimed into the piston bowl. The engine geometry is listed in Table 1, while a detailed schematic of the engine setup is seen in Fig. 1. More details for the experimental setup can be found in [27]. The usable range of HCCI for the engine was determined by Manofsky et al. [27] and is shown by the shaded region in Fig. 2. Experiments were performed at various fueling rates, indicated by lines in Fig. 2, and nvo was varied to control combustion phasing. Fuel was delivered with a single injection, starting at a crank angle 330° before top dead center combustion (TDCm). The fuel used was research-grade gasoline (90.5 RON, 82.6 MON). The usable HCCI operating range was limited by high CV (measured by the coefficient of variation, CoV, of IMEP) at late phasing and high ringing intensity (RI) at early phasing. In [27], these limits were chosen to a CoV of IMEP of 5% and a RI of 4 $\mathrm{MW/m^2}$. Note that the focus in the current work is on individual engine cycles and that these values are averages over many cycles only used to depict the feasible operating range. As indicated in Fig. 2, at low loads, a large
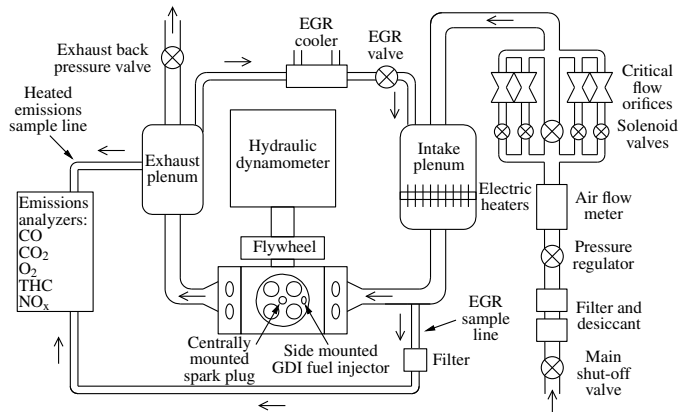

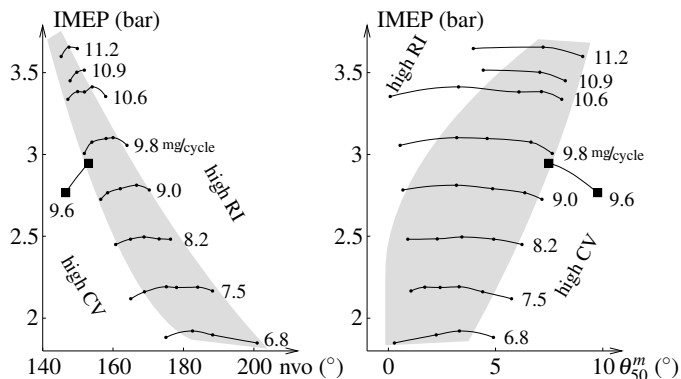Figure 1: Schematic of the FFVA engine experimental setup.

Figure 2: Usable HCCI operating range (shaded region) at 2000 rpm as determined in [27]. The data points analyzed in the present work are marked with squares.

range of nvo could be spanned before the limits of combustion were reached. However, at higher loads, slight changes in nvo had a greater effect on combustion. As fueling was increased, the limits of ringing intensity and CV converged and the operating range became narrower.

The analysis in the present work is focused on the two square points in Fig. 2, at fuel injection of 9.6 $\mathrm{mg/cycle}$, that transition from acceptable CV to higher CV. These conditions are a typical medium load operating point corresponding to net IMEP is approximately 2.8 bar with $\lambda = 1.7$. To fully observe and analyze the patters of cycle–to–cycle coupling, in-cylinder pressure

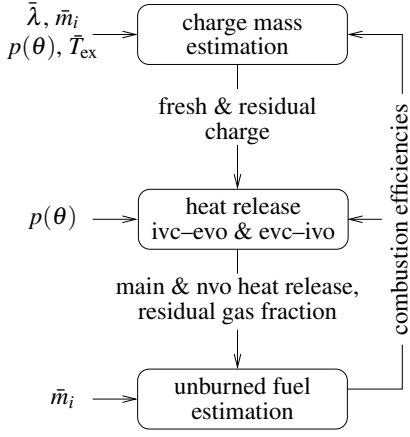| Component	Characteristic
Cylinders	1
Displaced volume	550 $\mathrm{cm^3}$
Stroke	94.6 mm
Bore	86.0 mm
Connecting rod	152.2 mm
Compression ratio	12.5:1
Number of valves	4
Piston shape	Shallow bowl
Head design	Pent-roof
Fueling method	Direct injection

Table 1: FFVA engine geometry.

Figure 3: Block diagram for the iterative estimation routine using measurements of $\lambda, m_i, p(\theta)$, and T_{ex}.
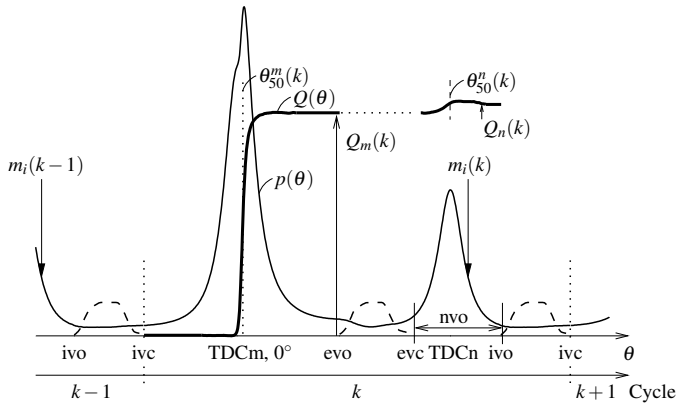

Figure 4: Definition of the engine cycle and important variables for typical curves of measured pressure $p(\theta)$, calculated heat release $Q(\theta)$, and known valve lift (dashed line).

was sampled at each crank angle degree for 3000 consecutive cycles. Nominal operating conditions for the experiments were 2000 rpm, controlled by a hydraulic dynamometer, and a coolant temperature that was controlled at 90°C. Analysis of points at lower and higher load were also done revealing that the same characteristics appear at these loads with the addition of runaway knock phenomena at higher loads.

DATA ANALYSIS

To analyze the experimental data an iterative estimation routine, depicted in Fig. 3, based on conservation of mass and energy is used. A novel method for estimating the mass of unburned fuel on a cycle basis is developed and combined with standard combustion analysis methods. The goal is to calculate the thermodynamic state, pressure and temperature, as well as variables important for explaining CV, such as unburned fuel and combustion efficiencies. The process is iterated until the values of combustion efficiencies converge at which point the governing relations of mass and energy conservation are satisfied.

The definitions of the engine cycle and important variables are given in Fig. 4 together with typical curves of measured pressure $p(\theta)$, calculated heat release $Q(\theta)$, and known valve lift. Note

that the heat release is calculated for both the main combustion event, between intake valve closing (ivc) and exhaust valve opening (evo), and the nvo period, between exhaust valve closing (evc) and intake valve opening (ivo). Top dead center main combustion is $0°$ and a new cycle starts at ivc. The total heat release in cycle k during main combustion and the nvo period are denoted by $Q_m(k)$ and $Q_n(k)$ respectively. In cycle k, the 50% burn angle where half the Q_m has occurred during main combustion is denoted by $\theta_{50}^m(k)$ and the corresponding angle during the nvo period is denoted by $\theta_{50}^n(k)$.

In the remainder of this section, the method for estimating the mass of unburned fuel on a cycle basis is derived. The other steps shown in Fig. 3 are based on standard methods and are described in detail in the Appendix.

UNBURNED FUEL   In order to model the mass of unburned fuel on cycle basis, a difference equation is derived for the unburned fuel mass that depends on known quantities and an initial unburned fuel mass. It is observed that the equation converges to the correct value given any initial guess. The model is subsequently used to estimate the combustion efficiencies.

The main combustion consumes a fraction $\eta_m(k)$ of the fuel mass and after the exhaust phase a fraction $x_r(k)$ of the residual gases is trapped. During re-compression a fraction $\eta_n(k)$ is further consumed so that, with homogeneous residuals, the unburned fuel mass carried over to the next cycle $k+1$ is

$$m_u(k+1) = x_r(k)\,(1 - \eta_m(k))\,(1 - \eta_n(k))\,m_f(k) \qquad (1)$$

where the fuel mass $m_f(k)$ in the beginning of cycle k is

$$m_f(k) = m_i(k-1) + m_u(k) \qquad (2)$$

with $m_i(k-1)$ being the injected fuel mass. The unknown combustion efficiencies in (1) are now related to the accumulated heat release. The gross heat released during main combustion Q_m is modeled by

$$Q_m(k) = m_f(k)\eta_m(k)q_{lhv} \qquad (3)$$

with q_{lhv} as the lower heating value for the fuel. As explained above, the fraction $\eta_m(k)$ of the fuel mass is consumed during main combustion and then the fraction $x_r(k)$ of the residual gases is trapped. Thus, the gross heat released during re-compression Q_n is given by

$$Q_n(k) = m_f(k)(1 - \eta_m(k))x_r(k)\eta_n(k)q_{lhv}. \qquad (4)$$

Combining Eqs. (1)–(4) yields a difference equation for $m_u(k)$ that can be iterated given an initial condition $m_u(0)$. The average value is used here for the fuel injection, i.e., $m_i(k) = \bar{m}_i$ since constant fueling was used in the experiments. The initial condition $m_u(0)$ is unknown but it can be shown that the series is convergent since x_r is between zero and one. The initial condition can be guessed and the result will be unique, after a transient, whatever the guess. The convergence rate depends on the value of x_r and, in this work, the value is about 40% which means that the influence of the true initial condition is reduced by a
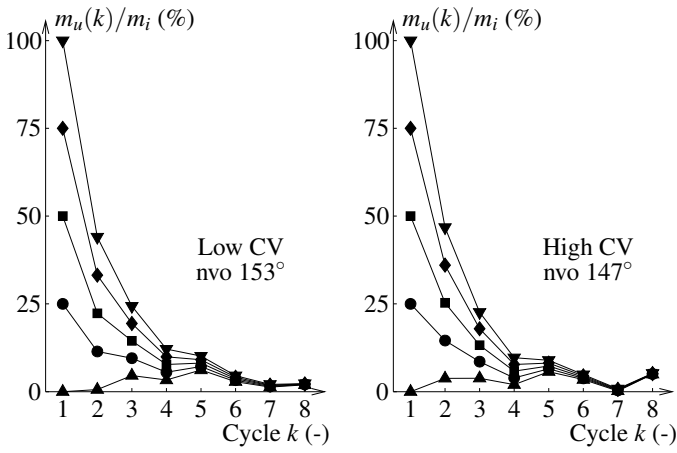
3

Figure 5: Convergence of the unburned fuel model is typically obtained in a few cycles. Shown here are the first cycles of one low-CV case (left) and one high-CV case (right).

factor of $0.4^8 < 1/1000$ after 8 cycles. The results are practically indistinguishable after this number of cycles for all cases starting from different initial conditions. This is demonstrated in Fig. 5 which shows the first iterations, starting from a range of initial conditions, for two cases. The approach adopted here is to guess $m_u(0) = 0$ and discard the first cycles in the analysis. Finally, when the unburned fuel mass is computed, (3) and (4) give

$$\eta_m(k) = \frac{Q_m(k)/q_{lhv}}{m_f(k)} \tag{5a}$$

$$\eta_n(k) = \frac{Q_n(k)/q_{lhv}}{x_r(k)\left(m_f(k) - Q_m(k)/q_{lhv}\right)} \tag{5b}$$

as approximations for the efficiencies which depends on the total gross heat releases (Q_m, Q_n) and residual gas fraction x_r. The computation of these quantities are based on standard methods and are described in the Appendix.

The proposed estimation of unburned fuel, based on the model (1), includes possible heat release during re-compression, the term $Q_n(k)$, which is neglected in previous low-order models associated with higher CV in HCCI–SI transients [28]. Simulation models with higher fidelity, including the effect of unburned fuel, are used in [25, 26] to study the effect of misfire in HCCI. In contrast, the aim here is to estimate the unburned fuel mass from experimental pressure data.

RESULTS

Observations from the data processing described in the previous section, applied on the measurements, are interpreted here. Results are shown for different nvo settings transitioning from lower to higher values of CV. The observations show that lean HCCI combustion with high CV is the result of unburned fuel passing over to the re-compression and to the next cycle which is supported by the following three important findings:

- There is a strong coupling and complementarity of the fuel burned during the main combustion and the re-compression events.
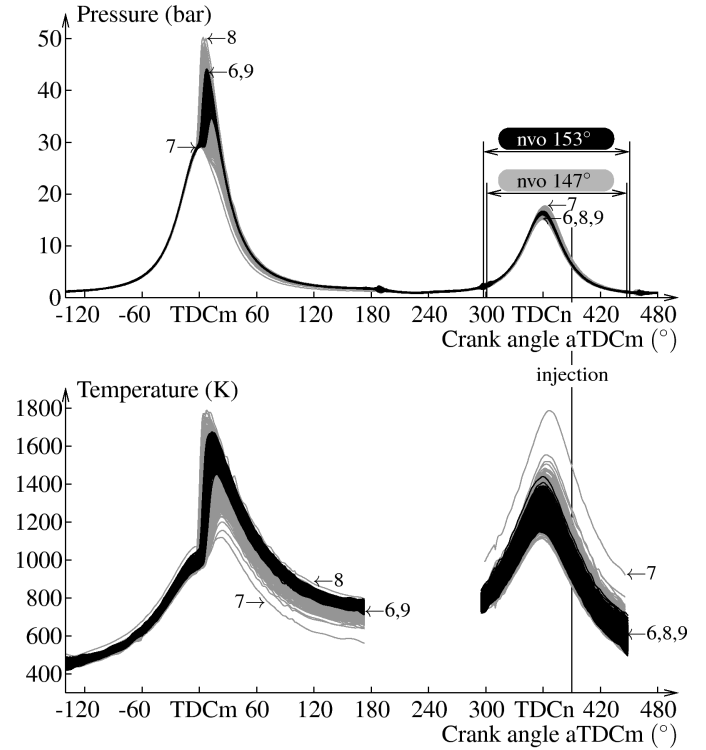

Figure 6: Measured pressure and calculated temperature for two different nvo settings with high and low CV. The numbered cycles are also marked in Fig. 7, 9, 13–15.

- Despite the complementarity, the available fuel does not necessarily burn during one cycle meaning that unburned fuel may carry over to the next cycle.

- Following a partial misfire, injection after TDC of re-compression does not necessarily cause combustion.

To explain and quantify these findings we highlight results from experiments with two nvo settings.

All the measured cylinder pressure traces for the two cases are shown in the upper half of Fig. 6. The lower part of the figure shows the charge temperatures computed from the heat release analysis. When reducing the overlap from 153° to 147° the average residual gas fraction reduces from 46% to 44% (see Fig. 17 in the Appendix). The average combustion phasing θ_{50}^m is pushed from 7.4° to 9.7° and the standard deviation is increased from 0.9° to 2.4°. The CoV of IMEP raises from a moderate 2.4% to a value of 13.3% which is typically considered above the acceptable limit. A few consecutive cycles are marked in Fig. 6, with the numbers 6 to 9, for the high CV case with nvo of 147°. These show, in the upper part of the figure, the peak pressure locations and, in the lower half, they identify the corresponding temperature traces. The same cycles are also shown in Fig. 7, 9, and in more detail in 13–15.

The spread of the attained pressures and temperatures generally increases when reducing nvo as shown in Fig. 6. Both lower and higher peak pressures and pressure rise rates are seen. The temperature during the re-compression does, however, mostly increase which suggests that if the temperature at evo is low,
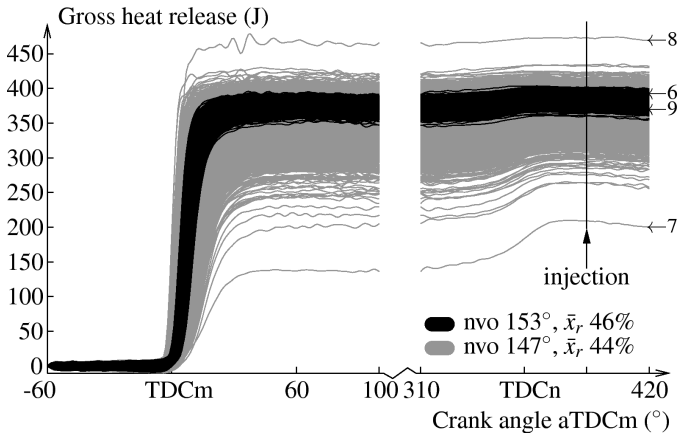
Figure 7: Accumulated gross heat release for two different nvo settings with high and low CV. The numbered cycles are also marked in Fig. 6, 9, 13–15.
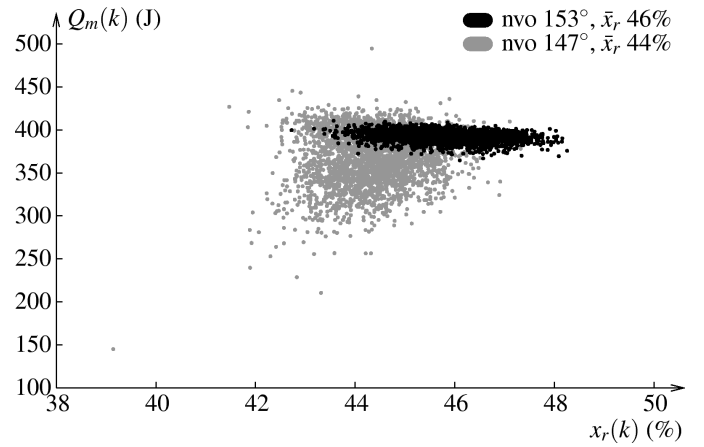

Figure 8: For high and low variability, the residual gas fraction $x_r(k)$ has no clear influence on the heat release $Q_m(k)$ during main combustion.

there is unburned fuel that will result in heat release during nvo. This connection will be made more clear later when discussing Fig. 9. The injection, starting at 30° after TDCn as marked in Fig. 6, has no visible effect on neither temperature nor pressure on the contrary to the simulation results in [25, 26] where, with a similar injection timing, combustion of all the available fuel is initiated.

The gross heat release traces for the two nvo settings are shown in Fig. 7. The traces for the case with low CV, in black, are tightly gathered and appear as one thick line whereas the larger variability is evident for the case with smaller nvo, in gray. The cycles with a low total heat release during main combustion, indicating a poor burn, have noticeable heat release occurring in the subsequent re-compression phase. The burn rates during re-compression for these cycles are rather slow, so a low efficiency is expected. Also, a number of cycles in the high variability case have higher total heat release than the ones observed in the low variability case. This indicates that unburned fuel carry over to the nvo period and to the next combustion cycle. Looking at cycles marked 6–9 in Fig. 6 and 7, reveals the same features. The sequence starts and ends with cycles with an evolution that looks similar to cycles in the low CV case. In between these well behaved cycles are two extreme cycles showing the effect of unburned fuel. Cycle 7 burns poorly and is followed by heat release and high temperatures in the nvo period. The eighth cycle has high peak pressure and high heat release during main combustion. Finally, there is no observable heat release in Fig. 7 associated with the injection. The results indicate that endothermic processes, due to vaporization and possibly pyrolysis, take place rather than combustion as suggested by the simulation results in [25, 26].

The estimates of the residual gas fraction x_r were found to be close to normally distributed (see the normal probability plot in Fig. 18 in the Appendix) indicating that the variability in x_r is random and without deterministic structure. The result in Fig. 8 further indicates that the variability in x_r has no clear influence on the heat release during main combustion Q_m. For the high CV case the cloud of points is moved to the left, since the mean x_r is

reduced, and stretched vertically, due to the higher variability in Q_m, but no trends appear.

In Fig. 9(a)–(d) the phasing $\theta_{50}^m(k)$ of main combustion, the temperature $T_{evo}(k)$ at evo, the heat release $Q_n(k)$ during the nvo period, and the temperature $T_{ivo}(k)$ at ivo are all plotted versus the heat release $Q_m(k)$ during main combustion in the same cycle k. Additionally, Fig. 9(e) and (f) show the phasing of the next cycle $\theta_{50}^m(k+1)$ and the unburned fuel in the next cycle $m_u(k+1)$ versus $Q_m(k)$. Figures 9(a)–(b) show that as nvo decreases and CV increases, late burns with low values of Q_m occur. These late cycles are associated with a lower temperature at evo and thus, here, the low combustion efficiency dominates the effect of late phasing on T_{evo}. With a lower Q_m there is a higher heat release Q_n during the subsequent nvo period as shown in Fig. 9(c). The end result is that a low Q_m is correlated with a higher temperature at ivo which is seen in 9(d). Figure 9(e) also shows that the increased residual charge temperature, through increased T_{ivo}, tends to advance the phasing of the next cycle $\theta_{50}^m(k+1)$. Figure 9(f) shows that, for the case with lower CV, the unburned fuel is approximately 0–6% of the injected fuel. For higher CV and particularly cycles with low $Q_m(k)$, the unburned fuel can reach up to higher values of approximately 10% of the injected fuel. Values up to 14% of the injected mass have been seen in an operating point with nvo of 145° and CoV of IMEP of 17.8%. In summary, $T_{evo}(k)$ decreases with decreasing $Q_m(k)$ but this effect is offset by $Q_n(k)$ leading to an increase in $T_{ivo}(k)$ and thus, the residual charge temperature of the next cycle increases and $\theta_{50}^m(k+1)$ advances. In addition, the unburned fuel mass carrying over to the next cycle is increased when the main combustion has a poor efficiency even though there is heat release during the re-compression. This chain of events is also evident for the sequence of cycles $k = 6, \ldots, 9$ marked in Fig. 9. The seventh cycle burns late with a low Q_m causing low T_{evo}. Some of the unburned fuel burns during nvo giving a high Q_n and increased T_{ivo}. The following cycle, number 8, has an early phasing and an unburned fuel of about 8% of the injected fuel mass, as shown in the bottom two plots. The bottom right plot also shows that during the eighth cycle with a high Q_m all the unburned fuel is depleted.

Note that the trends in Fig. 9(a) and (f) are reversed. A low $Q_m(k)$ in cycle k is correlated with a late phasing $\theta_{50}^m(k)$ but, as explained above, correlated with an early phasing $\theta_{50}^m(k+1)$ of the next cycle. It is thus crucial to have a clearly defined engine cycle when studying data from operating conditions with high CV.

The calculated $\eta_m(k)$, through Eq. (5a), versus combustion phasing $\theta_{50}^m(k)$ in main combustion is shown in Fig. 10. The spread in (θ_{50}^m, η_m) becomes larger with increasing CV and the mean of η_m has a negative trend with a sharp falloff when phasing is retarding. The peak combustion efficiency, the combustion timing where the efficiency starts to drop, and the rate with which the efficiency drops are features that are expected to vary and primarily depend on equivalence ratio and engine speed according

Figure 10: Combustion efficiency η_m and scaled averaged pressures for high and low CV. The efficiency decreases quickly with late combustion phasing θ_{50}^m.
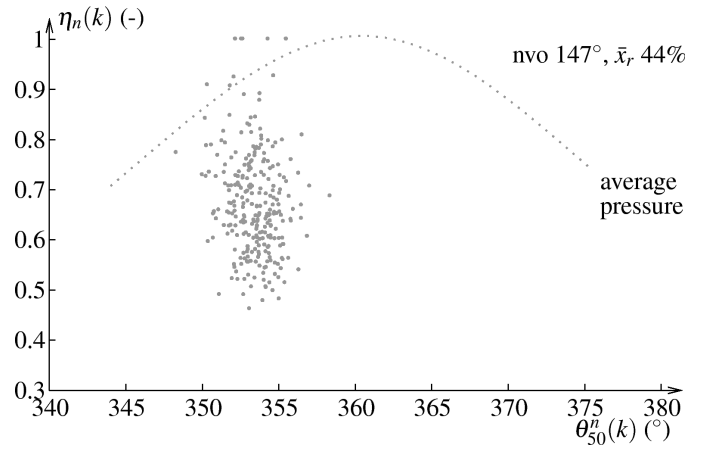
Figure 11: Combustion efficiency η_n versus the phasing θ_{50}^n during re-compression and a scaled averaged pressure.

to the experimental results in [29] and the computational fluid dynamics studies in [30]. These conditions are fairly constant for the operating conditions here but the relationship between efficiency versus phasing has the expected qualitative trend.

The computed $\eta_n(k)$, see Eq. (5b), are shown in Fig. 11 versus phasing during nvo $\theta_{50}^n(k)$ and in Fig. 12 versus the main combustion efficiency η_m (5a). Since η_n is undefined when there is negligible unburned fuel mass, only points where noticeable heat release occurs are plotted. Because of this, there are no points in Fig. 11 or 12 for the low CV case. For the combustion efficiency during the nvo period, there is no clear correlation with phasing in Fig. 11. Most of the cycles with significant heat release during re-compression have a rather early phasing of 4 to 10 degrees before top dead center and an efficiency of 50% to 80%. In Fig. 12, the majority of the points lies under the diagonal which shows that, when heat release occur during nvo, the efficiency η_n is typically lower than during the main combustion η_m. Note that more accurate estimates of the efficiencies can be obtained by analyzing gas samples on a cycle basis but with the current experimental setup we are limited to pressure-based analysis. Moreover, it is noted that the value of η_n is more challenging to estimate than η_m due to a lower signal (the heat release during re-
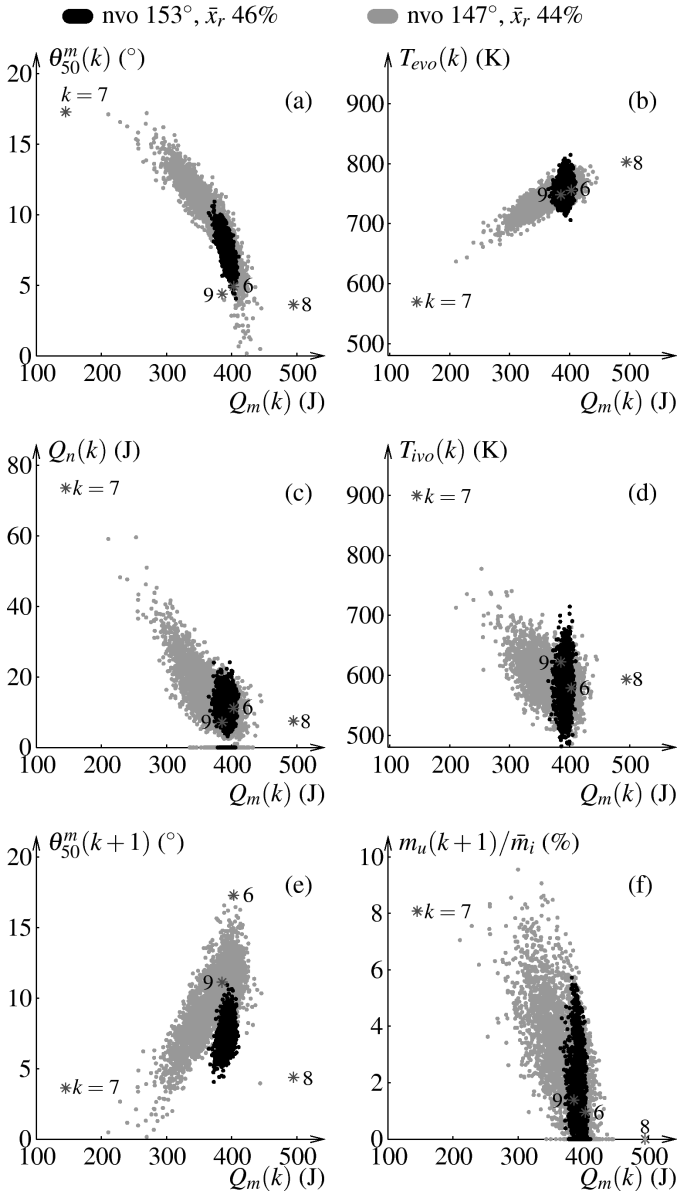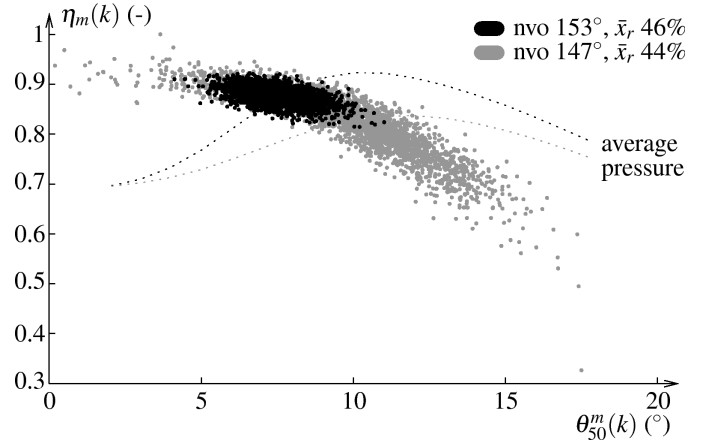

Figure 9: Heat release $Q_m(k)$ during main combustion versus combustion phasing $\theta_{50}^m(k)$ during main combustion, temperature $T_{evo}(k)$ at evo, heat release $Q_n(k)$ during the nvo period, temperature $T_{ivo}(k)$ at ivo, combustion phasing $\theta_{50}^m(k+1)$, and unburned fuel $m_u(k+1)$.
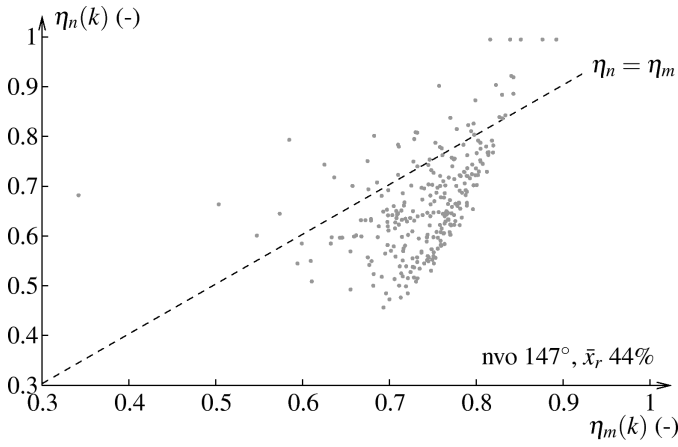
Figure 12: Combustion efficiency η_n during nvo versus efficiency η_m during main combustion for high CV.
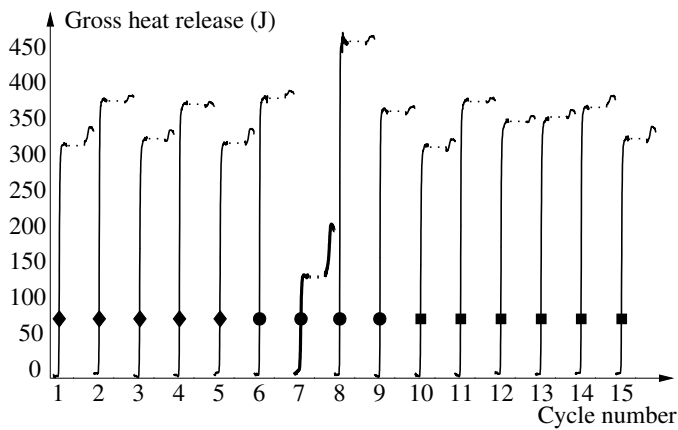

Figure 13: Gross heat release for consecutive cycles in conditions when the CV is high. The markers identify the corresponding cycles in 14. Cycles 6–9 are also shown in Fig. 6, 7, 9.
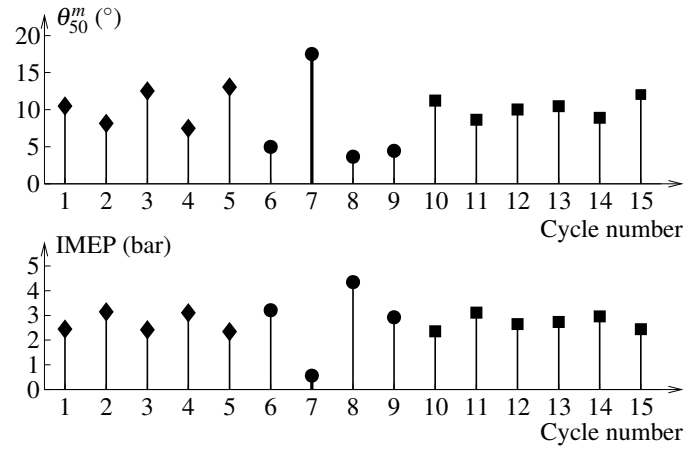

Figure 14: Combustion phasing and net IMEP for consecutive cycles in an operating condition with high CV. The markers identify the corresponding cycles in Fig. 13. Cycles 6–9 are also shown in Fig. 6, 7, 9.
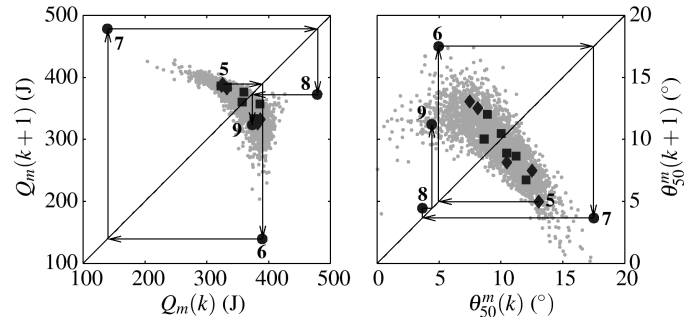

Figure 15: Return maps for the heat release Q_m (left) and the phasing θ_{50}^m (right). The markers identify the corresponding cycles in Fig. 13–14 and cycle $k = 5,\ldots,9$ are numbered.

compression) to noise ratio (noise in the pressure measurements and the accuracy of the heat transfer model).

CYCLE EVOLUTION   To study how the cycles evolve, when the CV is high, in some detail a few illustrative cycles are selected from the condition corresponding to an nvo setting of $147°$. After that, return maps are used to show that this qualitative behavior is indeed typical for this operating condition. Out of the 15 selected cycles, 6–9 were discussed also in the previous section, in connection with Fig. 6, 7, and 9. That perspective suggested that the sequence started and ended with seemingly regular cycles and in between there were two extreme ones with low and high heat release. However, studying the dynamical behavior in more detail reveals that there is a sequence of several cycles leading up to the extreme ones.

The gross heat releases for the 15 selected cycles are shown in Fig. 13, the combustion phasing and net IMEP are shown in Fig. 14. From the IMEP and the heat release traces it is seen that the first six cycles have approximately a period-2 cycle. All odd cycles have lower heat release during main combustion and higher during re-compression compared to the even cycles.

This leads to oscillations in the initial temperature which are transferred to the phasing and efficiency of the combustion. The combustion phasing oscillates with an increasing amplitude as seen in Fig. 14. Due to the fact that the combustion efficiency drops sharply when the phasing is late, as shown in Fig. 10, the increasing amplitude eventually leads to a particularly poor burn in the seventh cycle, marked with bold lines in Fig. 13–14. This leads to a heat release and a peak pressure, see Fig. 6, during nvo that are higher than previously. The following cycle has an early phasing due to the elevated initial temperature. Cycle 8 also has the largest heat release of all cycles which indicates an efficient burn, due to earlier phasing, of the injected fuel plus unburned fuel from previous cycles. The following cycle has an average heat release but an early phasing indicating that the initial temperature is elevated after the high heat release in the eight cycle. The two extreme cycles, 7 and 8, cause the combustion to recover and then, at least temporarily, continue with average values of phasing and heat release.

Figure 15 shows the return maps for the combustion phasing θ_{50}^m and the total gross heat release Q_m for all cycles at the operating point studied. The return map is a plot of the variable at cycle k versus the value at the next cycle $k+1$ and so reveals relationships between subsequent cycles. The 15 cycles from Fig. 13–14 are marked and the evolution of cycle 5–9 is traced with arrows.

The first cycles in this sequence alternate on either side of the diagonals in the return maps. As noted above, the heat release oscillates approximately between two values. The combustion phasing, however, oscillates with an increasing amplitude as seen in Fig. 14 and 15. Note that the pattern for the phasing of all cycles, the gray points in Fig. 15, stretches out with a slope close to negative one which suggests that this behavior appears repeatedly in the data. The unstable behavior is also seen in the vertical pattern in the return map for the heat release. This shows that, for a normal heat release value in one cycle the next one can have a large range of values. Due to the fact that the combustion efficiency drops sharply when the phasing is late, as shown in Fig. 10, an increasing amplitude will eventually lead to a significantly lower heat release as in the seventh cycle in the sequence. As explained above, this leads to significant nvo heat release and also high heat release during the next combustion cycle. These two extreme cycles cause the combustion to recover and then, at least temporarily, continue with average values of phasing and heat release. For the global patterns, this recovery behavior is shown by the bent tip for the phasing and the two other "legs", besides the unstable vertical direction, for the heat release.

CONCLUSIONS

Experimental data and combustion analysis results are presented for lean HCCI combustion, operated with nvo, with increasing levels of CV. Standard methods for combustion analysis are extended with a novel approach to estimate the mass of unburned fuel and combustion efficiency on a cycle basis for cases with high CV. The analysis is applied on the main combustion and the re-compression period which reveals important features for the understanding of CV. The results are summarized in the following three points.

- There is a strong coupling and complementarity of the fuel burned during the main combustion and the re-compression events.

- Despite the complementarity, the available fuel does not necessarily burn during one cycle meaning that unburned fuel may carry over to the next cycle.

- Following a partial misfire, injection after TDC of re-compression does not necessarily cause combustion.

The observations collectively show that quantifying the unburned fuel passing over to the re-compression and to the next cycle are essential in the understanding of high CV.

For conditions with high CV, unburned fuel carries over to the re-compression as well as to the next cycle. This causes heat release during nvo, affecting the charge temperature, and higher than average heat release and elevated temperatures during subsequent cycles. The recycled unburned fuel thus creates a coupling between cycles, in addition to the known coupling effect of temperature, that is essential to take into account in order to explain the behavior of CV. These nonlinear couplings between the recycled thermal energy in the residual gas and the recycled chemical energy in the unburned fuel mass are very important

for understanding, predicting, and eventually controlling HCCI combustion smoothly. Ongoing efforts [31] have also shown that if these dominating mechanisms are modeled, the observed behavior can be reproduced.

REFERENCES

[1] D. Law, D. Kemp, J. Allen, G. Kirkpatrick, and T. Copland. Controlled combustion in an IC-engine with a fully variable valvetrain. In *SAE World Congr.*, 2001. SAE 2001-01-0251.

[2] R.H. Thring. Homogeneous charge compression ignition (HCCI) engines. In *SAE Int. Fall Fuels and Lubr. Meeting and Exhibition*, 1989. SAE 892068.

[3] L. Koopmans and I. Denbratt. A four stroke camless engine, operated in homogeneous charge compression ignition mode with commercial gasoline. In *SAE World Congr.*, 2001. SAE 2001-01-3610.

[4] J.-O. Olsson, P. Tunestål, B. Johansson, S. Fiveland, R. Agama, and M. Willi. Compression ratio influence on maximum load of a natural gas fueled HCCI engine. In *SAE World Congr.*, 2002. SAE 2002-01-0111.

[5] L. Koopmans, O. Backlund, and I. Denbratt. Cycle to cycle variations: Their influence on cycle resolved gas temperature and unburned hydrocarbons from a camless gasoline compression ignition engine. In *SAE World Congr.*, 2002. SAE 2002-01-0110.

[6] S. Karagiorgis, N. Collings, K. Glover, N. Coghlan, and A. Petridis. Residual gas fraction measurement and estimation on a homogeneous charge compression ignition engine utilizing the negative valve overlap strategy. In *SAE World Congr.*, 2006. SAE 2006-01-3276.

[7] M. Sjöberg, J.E. Dec, A. Babajimopoulos, and D. Assanis. Comparing enhanced natural thermal stratification against retarded combustion phasing for smoothing of HCCI heat-release rates. In *SAE World Congr.*, 2004. SAE 2004-01-2994.

[8] D. Blom, M. Karlsson, K. Ekholm, P. Tunestål, and R. Johansson. HCCI engine modeling and control using conservation principles. In *SAE World Congr.*, 2008. SAE 2008-01-0789.

[9] J. Willand, R-G. Nieberding, G. Vent, and C. Enderle. The knocking syndrome–its cure and its potential. In *SAE Int. Fall Fuels and Lubr. Meeting and Exhibition*, 1998. SAE 982483.

[10] H. Persson, R. Pfeiffer, A. Hultqvist, and B. Johansson. Cylinder-to-cylinder and cycle-to-cycle variations at HCCI operation with trapped residuals. In *SAE World Congr.*, 2005. SAE 2005-01-0130.

[11] A. F. Jungkunz, H.-H. Liao, N. Ravi, and J. C. Gerdes. Reducing combustion variation of late-phasing HCCI with cycle-to-cycle exhaust valve timing control. In *IFAC Symp. on Advances in Automotive Control*, 2010.

[12] A. F. Jungkunz, H.-H. Liao, N. Ravi, and J. C. Gerdes. Combustion phasing variation reduction for late-phasing HCCI through cycle-to-cycle pilot injection timing control. In *Proc. of the ASME Dynamic Systems and Control Conference*, 2011.

[13] R. M. Wagner, K. D. Edwards, C. S. Daw, J. B. Green Jr., and B .G. Bunting. On the nature of cyclic dispersion in spark assisted HCCI combustion. In *SAE World Congr.*, 2006. SAE 2006-01-0418.

[14] C. S. Daw, R. M. Wagner, K. D. Edwards, and J. B. Green Jr. Understanding the transition between conventional spark-ignited combustion and HCCI in a gasoline engine. *Proc. Combust. Inst.*, 31(2):2887–2894, 2007.

[15] A. Ghazimirsaied, M. Shahbakhti, and C.R. Koch. HCCI engine combustion phasing prediction using a symbolic-statistics approach. *J. Eng. Gas Turbines Power*, 132(8): 082805, 2010.

[16] M. Sjöberg and J.E. Dec. Comparing late-cycle autoignition stability for single- and two-stage ignition fuels in HCCI engines. *Proc. Combust. Inst.*, 31(2):2895–2902, 2007.

[17] L. Xingcai, J. Libin, M. Junjun, and H. Zhen. Experimental study on the cycle-by-cycle variations of homogeneous charge compression ignition combustion using primary reference fuels and their mixtures. *Proc. Inst. Mech. Eng., Part D*, 221(7):859–866, 2007.

[18] M. Shahbakhti and C.R. Koch. Characterizing the cyclic variability of ignition timing in a homogeneous charge compression ignition engine fuelled with n-heptane/iso-octane blend fuels. *Int. J. Engine Res.*, 9(5):361–397, 2008.

[19] C.J. Chiang and A. G. Stefanopoulou. Stability analysis in homogeneous charge compression ignition (HCCI) engines with high dilution. *IEEE Trans. Control Syst. Technol.*, 15 (2):209–219, 2007.

[20] J.-M. Kang. Sensitivity analysis of auto-ignited combustion in HCCI engines. In *SAE World Congr.*, 2010. SAE 2010-01-0573.

[21] L. Koopmans, H. Ström, S. Lundgren, O. Backlund, and I. Denbratt. Demonstrating a SI-HCCI-SI mode change on a Volvo 5-cylinder electronic valve control engine. In *SAE World Congr.*, 2003. SAE 2003-01-0753.

[22] T. Urushihara, K. Hiraya, A. Kakuhou, and T. Itoh. xpansion of HCCI operating region by the combination of direct fuel injection, negative valve overlap and internal fuel reformation. In *SAE World Congr.*, 2003. SAE 2003-01-0749.

[23] H.H. Song, A. Padmanabhan, N. B. Kaahaaina, and C.F. Edwards. Experimental study of recompression reaction for low-load operation in direct-injection homogeneous charge compression ignition engines with n-heptane and i-octane fuels. *Int. J. Engine Res.*, 10(4):215–229, 2009.

[24] N. Wermuth, H. Yun, and P. Najt. Enhancing light load HCCI combustion in a direct injection gasoline engine by fuel reforming during recompression. *SAE Int. J. Engines*, 2(1):823–836, 2009.

[25] K.L. Knierim, S. Park, J. Ahmed, A. Kojic, I. Orlandini, and A. Kulzer. Simulation of misfire and strategies for misfire recovery of gasoline HCCI. In *Proc. American Control Conf.*, pages 3947–3952, 2008.

[26] C.G. Mayhew, K.L. Knierim, N.A. Chaturvedi, S. Park, J. Ahmed, and A. Kojic. Reduced-order modeling for studying and controlling misfire in four-stroke HCCI engines. In *Proc. 48th IEEE Conf. on Decision and Control*, pages 5194–5199, 2009.

[27] L. Manofsky, J. Vávra, D. Assanis, and A. Babajimopoulos. Bridging the gap between HCCI and SI: Spark-assisted compression ignition. In *SAE World Congr.*, 2011. SAE 2011-01-1179.

[28] C.S. Daw, K.D. Edwards, R.M. Wagner, and Jr. J.B. Green. Modeling cyclic variability in spark-assisted HCCI. *J. Eng. Gas Turbines Power*, 130(5):052801, 2008.

[29] Maximizing power output in an automotive scale multi-cylinder homogeneous charge compression ignition (HCCI) engine. In *SAE World Congr.*, 2011. SAE 2011-01-0907.

[30] Y. Mo. *HCCI heat release rate and combustion efficiency: A coupled KIVA multi-zone modeling study*. PhD thesis, University of Michigan, 2008.

[31] E. Hellström and A. G. Stefanopoulou. Modeling cyclic dispersion in autoignition combustion. In *Proc. 50th IEEE Conf. on Decision and Control*, pages 6834–6839, 2011.

[32] J.B. Heywood. *Internal Combustion Engine Fundamentals*. McGraw-Hill, 1988.

[33] J. Chang, O. Güralp, Z. Filipi, and D. Assanis. New heat transfer correlation for an HCCI engine derived from measurements of instantaneous surface heat flux. In *SAE Powertrain & Fluid Systems*, 2004. SAE 2004-01-2996.

[34] A. Babajimopoulos, P.Challa V. S. S., G. A. Lavoie, and D. Assanis. Model-based assessment of two variable cam timing strategies for HCCI engines: Recompression vs. rebreathing. In *Proc. ASME Internal Combust. Engine Div. Spring Tech. Conf.*, 2009.

[35] L. Eriksson. CHEPP – a chemical equilibrium program package for Matlab. *SAE Trans., J. Fuels Lubr.*, 4(113): 730–741, 2005.

[36] R.P. Fitzgerald, R.R. Steeper, J.A. Snyder, R.K. Hanson, and R.P. Hessel. Determination of cycle temperatures and residual gas fraction for HCCI negative valve overlap operation. *SAE Int. J. Engines*, 3(1):124–141, 2010.

[37] E. A. Ortiz-Soto, J. Vávra, and A. Babajimopoulos. Assessment of residual mass estimation methods for cylinder pressure heat release analysis of HCCI engines with negative valve overlap. In *Proc. ASME Internal Combust. Engine Div. Fall Tech. Conf.*, 2011.

APPENDIX: COMBUSTION ANALYSIS DETAILS

This appendix describes the components of the iterative estimation routine depicted in Fig. 3 that are based on standard methods for analysis of the measured cylinder pressure. Namely, the calculation of the heat release and the charge mass. The third component in Fig. 3, the computation of the mass of unburned fuel, was derived above. It is important to note that the heat release analysis is applied for both the main combustion period as well as the nvo period of the engine cycle. Figure 4 shows the definition of the engine cycle and important variables.

HEAT RELEASE   A heat release analysis is done and the results are used in estimating the unburned fuel as described above. The analysis, see Fig. 3, is based on pressure measurements together with the estimates of charge mass, residual mass, and combustion efficiencies. The combustion efficiencies were estimated above in Eq. (5) and the mass estimates are obtained by the method described in the next section. Initial values of combustion efficiencies are required for the first iteration of the process in Fig. 3 and these are selected as the average total value computed from exhaust measurements.

The computation of heat release follows standard methods for analyzing cylinder pressure data based on the first law of thermodynamics [32, Ch. 9.2]. The same analysis is applied on the main combustion as well as the nvo period with different values of total mass, unburned gas composition, and combustion efficiency. This approach is outlined below.

The released energy Q is governed by

$$\delta Q = \frac{1}{\gamma - 1} V dp + \frac{\gamma}{\gamma - 1} p dV + \delta Q_l \qquad (6)$$

where γ is the specific heat ratio, V is cylinder volume, and Q_l is heat loss which is governed by

$$\frac{dQ_l}{dt} = A h_c (T_{cyl} - T_w) \qquad (7)$$

where A is the chamber surface area and T_{cyl}, T_w are cylinder and wall temperature, respectively. The heat-transfer coefficient h_c is given by the modified Woschni relation derived in [33] and T_w is assumed to be constant and equal to 410 K [34]. The mass is assumed constant throughout the computation.

The properties $\gamma(\theta)$ and $R(\theta)$ are first assumed to be constant and equal to the values for unburned gas. Solving (6) and (7) gives the accumulated heat release $Q(\theta)$. The cylinder temperature is $T_{cyl} = pV/mR$ where m is m_t for the main combustion and m_r for the nvo period. The thermodynamic properties are then updated based on the mass fractions $y(\theta)$,

$$y(\theta) = (1 - x_b(\theta)) y_u + x_b(\theta) y_b(\theta)$$

where $x_b(\theta)$ is the mass fraction burned curve defined by

$$x_b(\theta) = \eta \, Q(\theta) \big/ \max_\theta Q(\theta)$$

with η being η_m for main combustion and η_n for nvo combustion. The fractions y_u and $y_b(\theta)$ represent the compositions of the unburned and burned gas respectively. The composition $y_b(\theta)$ is computed for chemical equilibrium at $(p(\theta), T(\theta))$. The equilibrium and the thermodynamic properties for a given composition can be found by chemical equilibrium software, e.g., [35]. This process is iterated until the values of the properties change less than a given tolerance. Finally, the total gross heat release during the main combustion and re-compression, denoted by Q_m and Q_n respectively, are given by

$$Q_m(k) = \max_{\theta \in (\text{ivc,evo})} Q(\theta)$$

$$Q_n(k) = \max_{\theta \in (\text{evc,ivo})} Q(\theta)$$

when the process has converged.

CHARGE MASS   The computation of the fresh charge mass uses the relative air-fuel ratio λ, determined from exhaust species measurements, and injected fuel mass m_i, measured by a flow meter, together with the estimate of unburned fuel m_u, see Fig. 3. The accurate determination of the fresh charge on a cycle basis is complicated and the most accurate method available for this work is relying on exhaust measurements sampled once every second. With lean combustion, small cyclic variations in air charge should have minor influence on the combustion in comparison to, e.g., the mass of unburned fuel. For these reasons, the fresh air charge inducted $m_a(k)$ is assumed to be equal for all cycles k and computed from the relative air-fuel ratio $\bar{\lambda}$, which correspond to an averaged value, according to

$$m_a(k) = \bar{\lambda} \bar{m}_i \text{AF}_s \qquad (8)$$

where AF_s is the stoichiometric ratio and $\bar{m}_i$ is the average value of the injected fuel mass.

The residual charge mass is determined from measurements of pressure p and exhaust temperature T_{ex} together with the estimate of combustion efficiency during main combustion η_m, see Fig. 3. The calculation follows the method in [36], with a few changes, described below. For a discussion about the accuracy and sensitivity of this method, please see [36, 37].

The mass flowing out from the cylinder in a cycle is the difference between the total charge mass m_t, trapped in the cylinder during main combustion, and the residual charge mass m_r, that remains trapped during the nvo period,

$$m_{out} = m_t - m_r. \qquad (9)$$

The mass flow out of the cylinder is assumed equal to the flow in

$$m_{in} = m_a(k) + \bar{m}_i \qquad (10)$$

during stationary conditions and neglecting blow-by. Using the ideal gas law for m_t and m_r, we have the equation

$$m_{in} = \frac{p_{evo}V_{evo}}{RT_{evo}} - \frac{p_{evc}V_{evc}}{RT_{evc}} \qquad (11)$$

with the unknowns being the temperatures T_{evo} and T_{evc}. In addition to the mass conservation (11), the exhaust process is approximated by an ideal gas undergoing a reversible process so that the heat lost per unit mass q_l is

$$q_l(\theta_0, \theta_1) = \int_{T(\theta_0)}^{T(\theta_1)} c_p\, dT - \int_{p(\theta_0)}^{p(\theta_1)} \frac{RT}{p}\, dp \qquad (12)$$

and the exhaust process is divided at a reference point θ_{ref} into a blow-down phase (BD) and a compression phase (CO). The ratio between the heat losses during the two portions of the exhaust phase, divided by θ_{ref}, is denoted by r_{ex},

$$r_{ex} = \frac{q_l(\theta_{evo}, \theta_{ref})}{q_l(\theta_{ref}, \theta_{evc})}. \qquad (13)$$

The point θ_{ref} is chosen in [36] as the point where cylinder pressure reaches 1 atm during the exhaust phase in between evo and evc. To ascertain that there always is a θ_{ref}, it is here instead chosen as the point of minimum pressure, denoted by p_{ref}, during the exhaust phase. With simplifications outlined in [36], Eq. (12) is written as

$$(c_p + a)T_{evo} + (c_p - b)r_{ex}T_{evc} = T_{ref}(c_p - a + (c_p + b)r_{ex}) \qquad (14)$$

where $a = \frac{1}{2}R\log\frac{p_{ref}}{p_{evo}}$ and $b = \frac{1}{2}R\log\frac{p_{evc}}{p_{ref}}$. The temperature T_{ref} at θ_{ref} is offset by ΔT from the measured average exhaust temperature $\bar{T}_{ex}$,

$$T_{ref} = \bar{T}_{ex} + \Delta T \qquad (15)$$

where ΔT is selected based on comparisons, in previous work, between results from the algorithm with simulation results from a GT-Power model of the engine [37]. The ratio r_{ex} is estimated based on convective heat transfer, governed by Eq. (7), where the cylinder temperature T_{cyl} is obtained by assuming polytropic processes. The coefficients h_c is taken from the modified Woschni relation derived in [33] and the wall temperature T_w is assumed constant. Combining (7) with (15) yields r_{ex} as a function of T_{evo} and T_{evc},

$$r_{ex} = f(T_{evo}, T_{evc}). \qquad (16)$$

The thermodynamic properties (c_p, R) in (11) and (14) are computed based on the mass fraction y_r

$$y_r = (1 - \eta_m)y_{re} + \eta_m y_{pr} \qquad (17)$$

where η_m is the combustion efficiency during main combustion and y_{re} and y_{pr} are the mass fractions for the reactants and products, respectively, calculated for each operating point.

In summary Eq. (11), (14), and (16) are three equations containing the three unknowns T_{evo}, T_{evc}, and r_{ex} that can be solved iteratively. The computed r_{ex} for each cycle are plotted in Fig. 16 showing that the mean is slightly decreasing and the spread
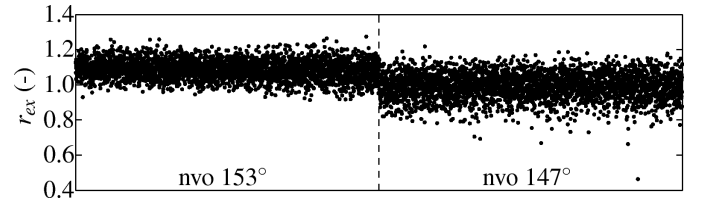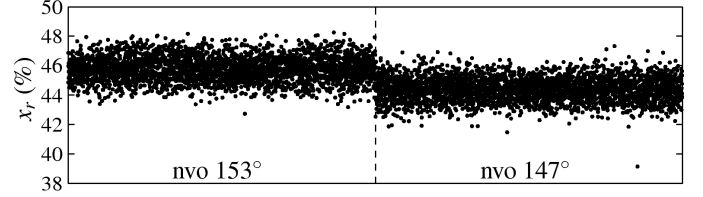

Figure 16: Heat transfer ratio r_{ex}.

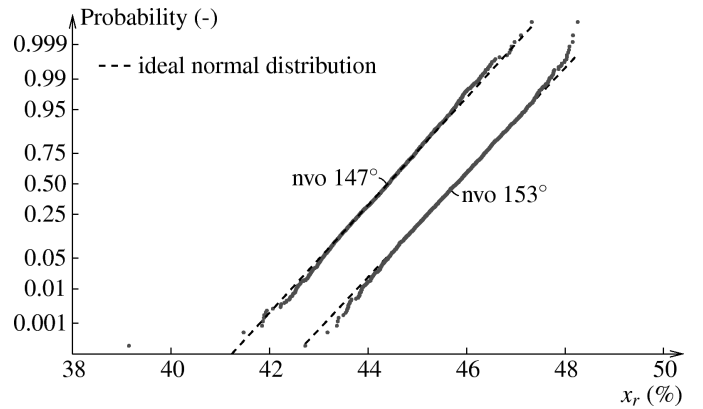Figure 17: Residual gas fraction x_r.

Figure 18: Normal probability plots of the residual gas fraction estimates.

increases somewhat as nvo decreases and CV increases. A sensitivity analysis by Fitzgerald et al. [36] showed that 20% error in r_{ex} causes errors less than 0.5% in the temperatures and thus, the influence on the estimates of T_{evo} and T_{evc} from the variability in r_{ex} shown in Fig. 16 is low.

When the solution $(T_{evo}, T_{evc}, r_{ex})$ is found, the charge mass m_t and residual charge mass m_r are computed from the ideal gas law and the residual gas fraction is approximated by

$$x_r(k) = \frac{m_r}{m_t} = \frac{p_{evc}V_{evc}}{p_{evo}V_{evo}}\frac{T_{evo}}{T_{evc}}. \qquad (18)$$

The estimates of x_r are shown in Fig. 17. The mean value $\bar{x}_r$ decreases with nvo and the standard deviation is approximately 0.8% for both cases. In the normal probability plot in Fig. 18 the values cluster close to a straight line implying that the estimates are close to a normally distributed and, hence, that there are almost no deterministic relationships between values of x_r.